Thermal loads in gaps between ITER divertor monoblocks: first lessons learnt from WEST

J.P. Gunn, J. Bucalossi, Y. Corre, M. Diez, E. Delmas, N. Fedorczak, A. Grosjean, M. Firdaouss, J. Gaspar, T. Loarer, et al.

Thermal loads in gaps between ITER divertor monoblocks: first lessons learnt from WEST

J. P. Gunn, J. Bucalossi, Y. Corre, M. Diez, E. Delmas, N. Fedorczak, A. Grosjean, M. Firdaouss, J. Gaspar,[a] T. Loarer, M. Missirlian, P. Moreau, E. Nardon, C. Reux, M. Richou, E. Tsitrone, and the WEST team[b]

CEA, IRFM, F-13108 Saint-Paul-Lez-Durance, France.

[a] Aix Marseille Univ, CNRS, IUSTI, Marseille, France

[b] See http://west.cea.fr/WESTteam

Corresponding author's e-mail adress: Jamie.Gunn@cea.fr

Abstract

In the WEST tokamak, ITER-like divertor targets consisting of tungsten monoblocks bonded via an OHFC-Cu compliance layer to CuCrZr cooling tubes were exposed to plasma during the 2018 experimental campaign in which modest heating power was available. Up to 2.5 MW/m^2 divertor surface heat flux was attained. Inspection of the components after the campaign revealed a wide variety of damage at both leading and trailing monoblock edges, and at the optical hot spots which are the projections along magnetic field lines of the toroidal gaps between monoblocks onto the poloidal leading edges. Cracking, deformation, and melting occurred. Consideration of the large body of past work on high heat flux testing, combined with the expected loading conditions in WEST, suggests that fractures form during the first transient events such as disruptions. Deformation occurs under subsequent exposure to steady state heat loads. Nearly identical damage was observed on reciprocating probes made of W-La(10%) alloy under measured irradiation conditions, lending credence to this hypothesis.

1   Introduction

The ITER divertor will consist of tungsten monoblocks (MB) bonded to poloidally-running CuCrZr cooling tubes, with ~0.5 mm toroidal gaps between them. Assessing what the thermal loads in gaps could be is a key point for the safe operation of the divertor in ITER because gaps introduce sharp edges onto which plasma influx will be focused, leading to intense local overheating inducing tungsten recrystallization, melting, and consequently, potential limitations on divertor lifetime [1]. Experimentally evaluating the evolution of ITER-like plasma-facing units (PFU) in a realistic fusion reactor environment is one of the

1

main missions of the WEST tokamak [2] and complements both theoretical calculations and tests in high heat flux facilities.

The WEST divertor is a flat, open design with no central dome. It is divided into 12 sectors each composed of 38 poloidally-running PFUs with width varying between 26 and 31 mm in the toroidal direction. The toroidal width varies poloidally because the divertor is tilted in the poloidal plane, and thus its nominal plasma-facing surface is conical. The phase I divertor, in operation since December 2016, is mostly composed of uncooled W-coated, graphite PFUs with 1° toroidal bevels to protect poloidal leading edges [3]. Some of them were equipped with Langmuir probes [4], thermocouples, and novel optical fibers equipped with Bragg gratings [5,6]. This exhaustive suite of diagnostics provides a powerful tool for estimating the heat flux to the divertor in the steady state, flat top phase.

During the third WEST experimental campaign in the second half of 2018 (referred to as the C3 campaign), one of the lower divertor sectors was partially equipped with 12 actively cooled ITER-like PFUs provided by three different suppliers (3 from China, 3 from Japan, and 6 from Europe), each of which has 35 MBs (Figure 1) of 12 mm poloidal width separated by 0.5 mm toroidal gaps. They were monitored by a very-high-resolution infrared camera (3.9µm wavelength, minimum temperature threshold ~300°C, 0.1 mm/pixel) [7]. The ITER-like PFUs were not beveled; some of them had 1 mm chamfers at both leading and trailing edges, while others had sharp edges. While most of the PFUs were aligned within the ITER tolerances (at most ±0.3 mm perpendicular steps between neighbouring PFUs), three of them were not: for example, at the outer strike point (OSP) PFU#7, PFU#12, and PFU#19 were measured to protrude respectively +0.31 mm, +0.79 mm, and +0.63 mm above their neighbours (Figure 2).
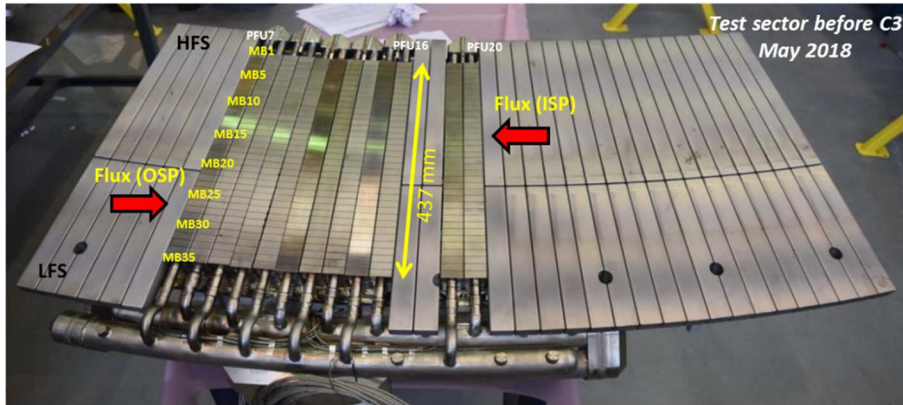

Figure 1. Photograph of the WEST lower divertor sector that was equipped with 12 ITER-like PFUs for the C3 experimental campaign. PFUs are numbered from 1 to 38 running in the toroidal direction (from left to right on the image), and the MBs are numbered from 1 to 35 running in the poloidal direction from the HFS to the LFS. The poloidal length of the ITER-like PFUs (437 mm) is indicated. The remaining PFUs are made of graphite with a 15 µm coating of W. The direction of the parallel heat flux is indicated at the inner and outer strike points (ISP and OSP).
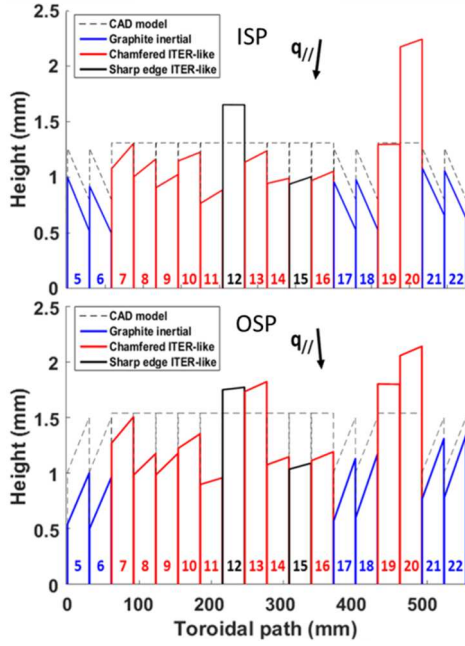
Figure 2. Representation of the results of a metrology study before the C3 experimental campaign illustrating the misalignments of the PFUs with respect to their nominal positions (dashed lines). The beveled graphite PFUs are shown in blue, the chamfered W PFUs are in red (the chamfers are not shown here because the exaggerated vertical scale does not yield a useful image), and the W PFUs with sharp edges are in black. These toroidal profiles are centered on MB#17 at the ISP (upper panel), and on MB#25 at the OSP (lower panel). Note that the vertical scale is greatly exaggerated in order to clearly show the misalignments.

During the C3 experimental campaign, significant progress was made in improving plasma performance. A total of 2h30 plasma exposure was cumulated over 1076 discharges, corresponding to a total injected energy of 5 GJ. The maximum plasma current was 818 kA, and the maximum discharge duration was 37.5 s. Auxiliary heating was mostly provided by lower hybrid antennas, coupling a maximum of 5.3 MW to the plasma. The maximum steady state surface heat load was $q_{pk} \sim 2.5$ MW/m^2 corresponding to parallel heat flux of $q_{//} \sim 50$ MW/m^2 for a typical B-field incidence angle of $\sim 3°$ at the outer strike point. There was a large number of disruptions (730) and many discharges had significant magnetohydrodynamic (MHD) activity, both of which can deliver intense transient heat pulses to plasma-facing components (PFCs) having durations of the order of a few ms.

2   Visual inspection after the C3 experimental campaign

The ITER-like PFUs were inspected under an optical microscope following the C3 experimental campaign [8]. Observations were made of a variety of damage on the PFUs including cracking, melting, and in particular clear evidence of optical hot spots (direct plasma impact on poloidal leading edges of MBs through toroidal gaps), predicted to occur in ITER [9]. The damage is observed on the full poloidal extent of the divertor, even on zones that normally should receive little or no heat flux in steady state. This paper will focus on PFU#12 (provided by the European Domestic Agency) which was the most poorly aligned (+0.79 mm) and which has sharp leading edges. Similar damage was also observed on chamfered PFUs [8] but will not be discussed here.

2.1   A bulk melting event

A detailed survey of the damage to PFU#12 is compiled in Figure 3. During the flat top phase, and depending on the X-point height, the outer strike point (OSP) can impinge on the left hand side of MBs 23 to 28, and the inner strike point on the right hand side of MBs 14 to 17. Despite being on the trailing edges of MBs 13 to 16, a significant amount of melting was observed there half way through the C3 campaign by the robotic articulated inspection arm that can penetrate into the tokamak and take photos under vacuum [10]. Melt layer motion and splashing of liquid W were clearly observable. Similar localized damage was not observed on any other PFUs. Furthermore, at the end of the campaign (Figure 4), the zone showed no evidence of evolution, leading us to believe that it was induced by a single event. The impact on the trailing edge of the MBs suggests that perhaps a disruption or even an impact of runaway electrons was responsible during the final instants when the magnetic equilibrium was collapsing. There was no evidence that the presence of this damage hindered the experimental campaign. Indeed, we were unable to find any precise data that would indicate when it occurred.
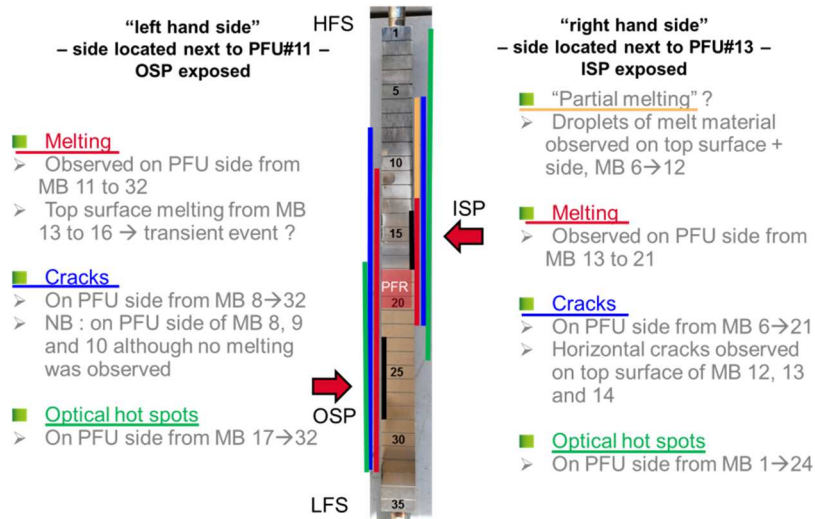

Figure 3. Summary of observed damage on misaligned PFU#12. The zones where the strike points impacted the divertor are indicated by black bars. Red bars indicate MBs on which leading edge melting occured. Blue bars indicate the presence of cracks (mostly vertical but some horizontal). Green bars indicate clear evidence for optical hot spots.
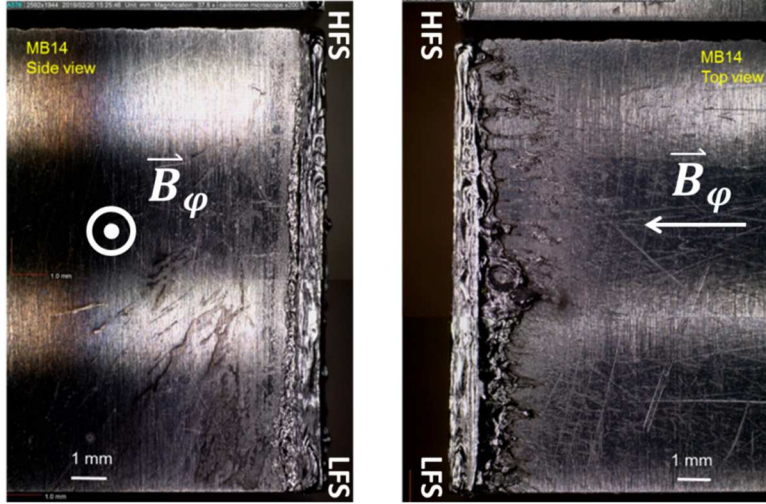
Figure 4. Side (left panel) and top (right panel) views of the trailing edge of MB#14. The images were taken after dismounting PFU#12 following the C3 experimental campaign. Melting of the leading edge to a depth about 1 mm and splashing of the melt layer over a few mm on the top surface are observed.

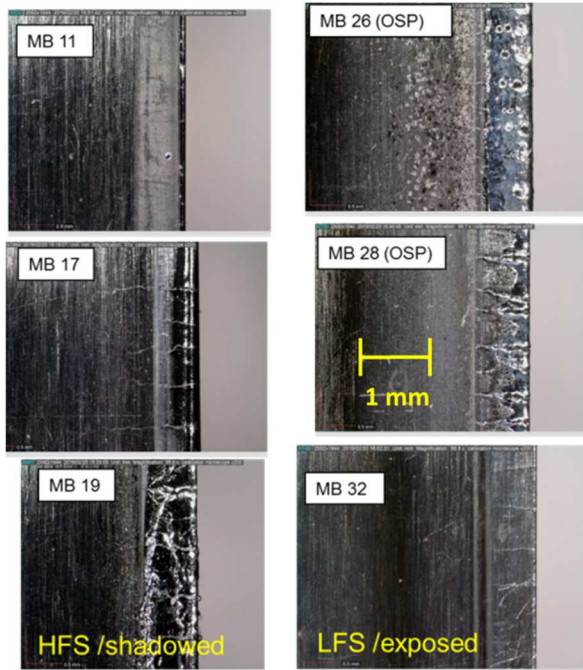## 2.2 Cracks and fine scale melting on exposed leading edges

Figure 5. Images of MBs on the left hand side of PFU#12. The discoloured band is 0.8 mm wide and corresponds to the misalignment of the PFU with respect to its neighbour, PFU#11. Cracks (mostly vertical) and deformation (or perhaps fine scale melting, to be confirmed) are observed. The crack density and the severity of the deformation/melting decrease towards the extremities of the affected zone, and seem to be the most severe at the location of the OSP. See Figure 1 for the locations of the MBs on the PFU.

Excluding the localized zone where an exceptional melting event occurred, the leading edges from MB#8 to MB#32 on the left hand side of the PFU show a number of interesting features (Figure 5). On the front faces of the MBs, a discoloured band ~0.8 mm high is visible. This corresponds exactly to the misalignment of PFU#12 with respect to its neighbour, PFU#11. There are a number of vertical cracks that often extend to the bottom of the plasma-wetted surface, but sometimes penetrating deeper into the shadowed area. The cracks are separated typically by 0.2 to 1.0 mm in the poloidal direction. The crack density is lower at the poloidal extremities of the affected area, and higher around the OSP location. Small scale melting is observed from MB#11 to MB#32 (again, excluding MB#13-16 where the severe melting event occurred). At the poloidal extremities of the damaged region the melting seems to be limited to the sharp leading edge, whereas towards the center of the

region, both on HFS and LFS MBs, the melting can occur over the entire depth of the exposed surface, notably along the edges of the cracks. It seems that the damage is maximal at the leading edges around the OSP, but it exists even on the trailing edges of MBs at the ISP (both being on the left hand side of the PFU). During start-up and ramp-down, and during disruptions, the strike points sweep poloidally and can lead to heat flux transiently striking the MB trailing edges. That is, during transient movements of the strike points, trailing edges that are nominally shadowed during the flat top phase can briefly become leading edges with respect to the heat flow.

At the top surface the same cracks that are observed on the front surfaces of the MB leading edges are observed to propagate up to ~0.5-1 mm in the toroidal direction (Figure 6). The geometry of the loaded leading edges has changed. It is not possible to conclude whether the volume of metal between the cracks has migrated in the toroidal and poloidal directions, forming a pattern of corrugation, or whether material at the crack locations has gone missing. The poloidal separation between the cracks is very regular, about 0.4 mm on average (there are 31 columnar structures over the 12 mm poloidal MB width). The PFUs were again exposed during the C4 experimental campaign in 2019 and shall be inspected to see how the cracks evolved.
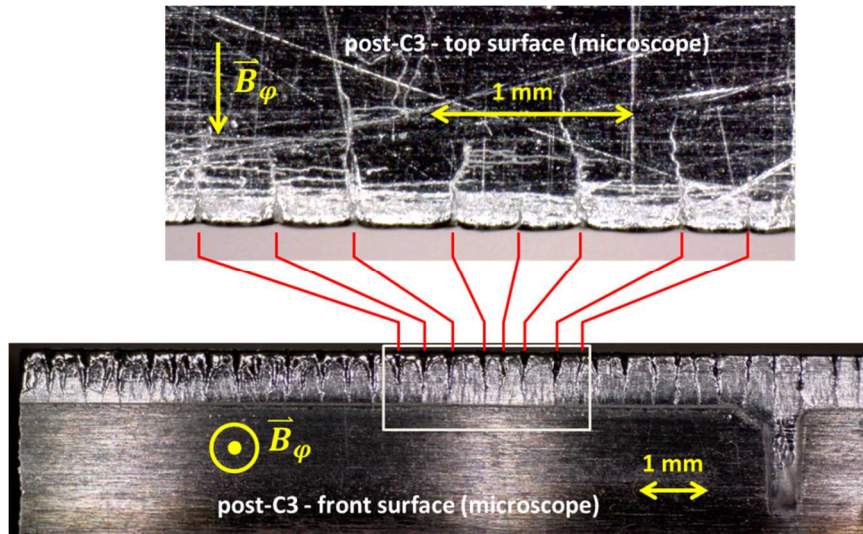

Figure 6. The upper panel is a microscope image of a part of the top surface near the exposed leading edge of MB#29 (left hand side, near OSP). An image of the full poloidal width of the leading edge is shown on the lower panel. Both images were taken after the 2018 (C3) experimental campaign.

At the right hand side of the PFU around the ISP location (Figure 7), there is also cracking and what appears to be fine scale melting, although the crack density and deformation of the surface are qualitatively less important than at the OSP location (Figure 5). At the leading edges of the MBs that were impacted by the exceptional melting event on their trailing edges, there appear to be metal droplets sticking to the plasma-wetted area.
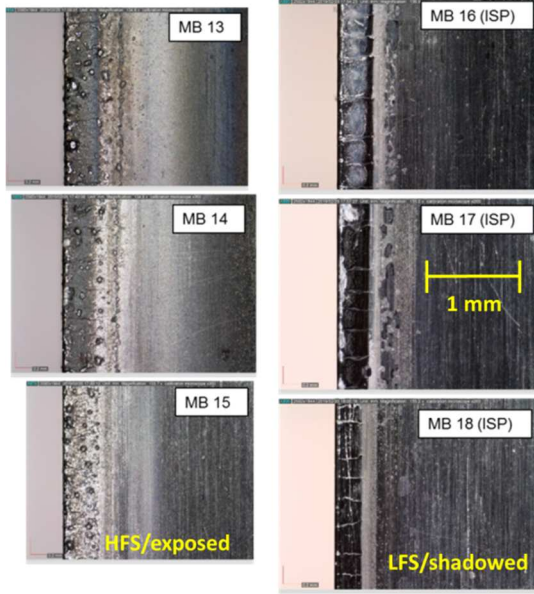
Figure 7. Side images of MBs on the right hand side of PFU#12, at the ISP. The discoloured band corresponds to the misalignment of the PFU with respect to its neighbour, PFU#13. Vertical cracks and fine scale melting are observed. On the leading edges of MBs#13-15, that were severely melted at their trailing edges, there appear to be droplets of liquid metal that stuck to the plasma-wetted area. See Figure 1 for the locations of the MBs on the PFU.

2.3   Optical hot spots on exposed leading edges

Charged particles propagating along magnetic field lines can penetrate through the toroidal gaps between MBs and strike the leading edge of the downstream PFU at near normal incidence, leading to localized spots of intense heat flux. The image of the gaps on the leading edge, calculated by field line tracing, are known as "optical hot spots" (OHS). Modelling predicts that in ITER, hot plasma released from the pedestal during ELMs could trigger flash melting or even W boiling at the OHSs, depending on the plasma scenario and the alignment of the MBs with respect to each other [9]. Numerical studies are important and contribute to improving the future divertor designs by proposing optimization solutions such as MB shaping [11,12]. The results presented in [8] and discussed in more detail here comprise the first experimental evidence for OHSs.

Figure 8 contains a remarkable image of the left-hand corner of MB#1 at the HFS extremity of PFU#12. A perfect image of its upstream neighbour, PFU#13, is visible, as if the image had been captured on an old-fashioned photographic plate from the nineteenth century. The gray band and the triangular protrusion at the top of the image represent surfaces to which magnetic field lines connect from the SOL, and along which plasma can arrive to impact the leading edge. In ITER, the upper band would not be visible due to the 0.5 mm toroidal bevel, but the triangular imprint, the OHS, will be [9,12]. The trailing faces of MB#1 and MB#2 of PFU#13 (dark bluish squares) as well as the interior of the toroidal gap (lighter gray) between them can be seen. The differences in aspect are likely related to the different origins of particles striking the surface (for example neutral particles reflecting from the trailing edges of the upstream MBs versus neutrals reflecting from inside the walls of the toroidal gap). To appreciate the image, the reader can imagine being a microscopic observer inside the poloidal gap between the PFUs, and looking along the magnetic field lines from PFU#12 towards PFU#13. The view is similar to the photo a tourist might take looking down a city street between two skyscrapers.
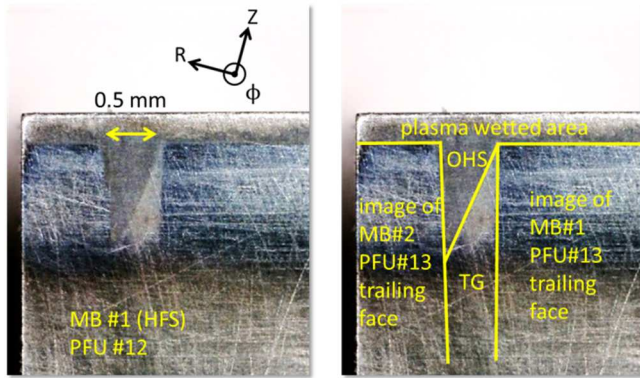
Figure 8. Photograph of the leading edge of MB#1 (the first MB on the HFS of PFU#12). The plasma heat flux is directed into the page. The image is repeated on the right panel, with lines indicating the MB edges to guide the eye. This deposition pattern is akin to a true photograph, and shows an image of what a microscopic observer would see looking along the field lines through a toroidal gap between MBs. The OHS is the triangular region.

On most MBs the OHS is visible, even in regions such as MB#1 where very little plasma flux is expected. In regions nearer the strike points where cracks and fine scale melting were observed on the exposed leading edges, the OHSs in many cases are also damaged. Cracks often descend vertically through the full depth of the OHS (Figure 9), and horizontal cracks branch out from them in some cases.
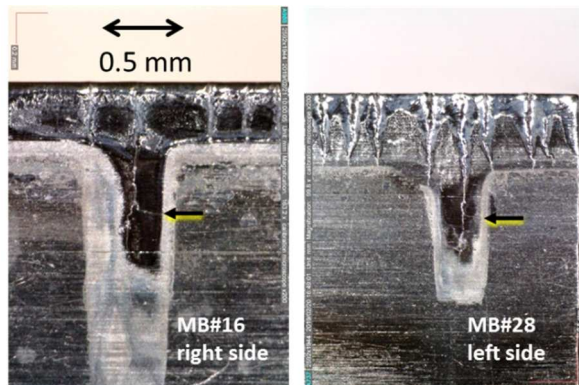

Figure 9. Examples of optical hot spots on the leading edge of MB#16 (right hand side, near ISP) and MB#28 (left hand side, OSP). The plasma heat flux is directed into the page in each case. There appears to be deformation at the edges of cracks on the exposed leading edge. Cracks extend down into the OHSs , and branching horizontal cracks are also seen (indicated by arrows).

2.4 Could the damage be caused by transient heat loads?

Early on it was recognized that thermal shock loading of pure sintered W below the ductile-to-brittle transition temperature (DBTT) results in brittle fracture formation [13]. Experiments were usually aimed at studying the effect of intense transient heat loads due to ELMs, disruptions, and vertical displacement events, involving energy fluences expected in ITER, and were so intense that they would typically provoke surface melting, particle ejecta, or even boiling. The melt layer, as it cools below the DBTT, experiences stress which may generate cracks. For example in [14], on W samples having initial temperature below the DBTT, grain boundary macro cracks accompanied by a network of fine cracks were observed after irradiation by the VIKA-93 hydrogen plasma gun with an energy fluence of 7.5 MJ/m^2 for up to 360 µs (heat flux factor = 400 MW m^{-2} s$^{1/2}$). The heat flux factor is defined as the incident heat flux multiplied by the square root of the exposure time for a constant heat pulse.

It is an engineering parameter, derived from the semi-infinite 1D heat conduction model, that provides an estimate of the surface temperature increase resulting from a transient heat pulse [15]. As a reference, an energy fluence of 1.0 MJ/m^2 is sufficient to cause shallow surface melting of W (see Figure 41 of [9]). For temperatures above the DBTT under the same loading conditions only fine surface cracks were observed. It was deemed essential that plasma-facing components made from pure sintered W be heated above the DBTT for use in a fusion reactor to avoid this severe brittle cracking [16]. Due to the expected embrittlement of W (increase of the DBTT) under neutron irradiation, efforts continue to find W-based materials with lower DBTT [17].

Brittle fractures also occur for lower heat loads that do not cause melting, but there is evidence that there is an energy threshold below which brittle fracturing does not occur on W samples having temperatures below the DBTT. In one study [18] of pure W with longitudinal grains running parallel to the irradiated surface (which corresponds exactly to the configuration of the leading edges of WEST MBs, with the grain elongation in the direction from the top surface downwards towards the cooling tube), the threshold was found to be ~200 MW/m^2 for an irradiation time of 1 ms, corresponding to a heat flux factor of merely 6 MW m^{-2} s$^{1/2}$. In another study of ITER-grade W heated to 200°C (still below the DBTT) [19], macro cracks were observed to form for single heat pulses as low as 150 MW/m^2 for 5 ms (heat flux factor = 11 MW m^{-2} s$^{1/2}$), but in that case the grains were oriented perpendicular to the surface. At preheating temperatures above the DBTT macro cracks did not appear. It was concluded that to provide safe operating conditions in fusion reactors, limiting brittle fracture formation, the base temperature of W PFCs has to be higher than the DBTT. Similar investigations [20] found that the DBTT of recrystallized W can be significantly higher than sintered W, and that brittle crack formation in general follows the grain boundaries with the possibility of cracks forming parallel to the surface at depths of 200-600 µm, which degrades the heat conduction properties of the material.

The mechanism responsible for brittle cracking is as follows [18]. A heat pulse causes the temperature of the near surface to rise above the DBTT allowing it to become ductile, while the material immediately below it remains brittle. Constrained by the colder material below, the hot surface layer can undergo plastic deformation. After the heat pulse, the hot layer cools back down below the DBTT almost instantly and returns to its brittle state, this time experiencing tensile stress as it tries to return to its original volume. If the tensile stress exceeds the yield strength, the material cracks. 2D thermal simulations of a heat pulse just below the brittle cracking threshold observed in JUDITH-1 [18] are shown in Figure 10. The temperature at the leading edge, and 0.1 and 0.2 mm into the bulk are shown. The thermal response was calculated by the simple finite difference model introduced in [9,12]. The model assumes the temperature-dependent thermal properties of tungsten adopted by ITER. Each
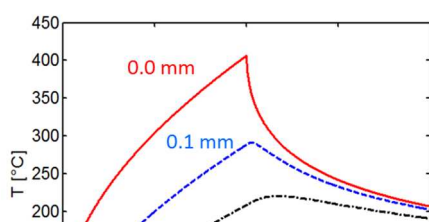

Figure 10. Thermal response of a 0.8 mm exposed leading edge to a square heat pulse of 190 MW/m^2 applied for 1 ms (heat flux factor = 6 MW m^{-2} s$^{1/2}$). The temperature at the surface (0.0 mm, full curve) and at two depths below the surface (0.1 mm, dashed curve; 0.2 mm, dot-dash curve) are shown. The initial temperature is 70°C.

tungsten grade has different properties depending on its production route, composition, purity, microstructure, thermal/irradiation history, and so on, so these calculations should only be taken as qualitatively illustrative. A broad range of DBTT can be found in the literature, from as low as 250°C [21] but not exceeding 500°C [22]. As a concrete example, a study of the mechanical properties of hot rolled versus hot forged W for the European Spallation Source [23] reported that the ductility of hot rolled W is greater than that of hot forged W. The DBTT was found to be 250-300 °C for the former and about 350 °C for the later. We shall assume the DBTT to be in the range 250-350°C in what follows.
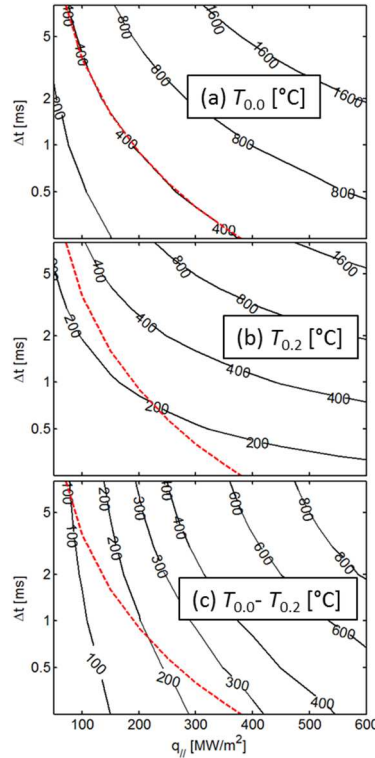

Figure 11. Thermal response of a 0.8 mm exposed leading edge to a square heat pulse as a function of parallel heat flux and exposure time. The dashed curve corresponds to a constant heat flux factor of 6 MW m^{-2} $s^{1/2}$ which is the threshold for brittle crack formation deduced in [18]. (a): Peak surface temperature. (b): Peak temperature at a toroidal depth of 0.2 mm from the leading edge. (c): The difference between (a) and (b).

Returning to Figure 10, the surface temperature rises to 400°C, just slightly above the DBTT, so it is perhaps consistent that cracking was not observed under those loading conditions in JUDITH-1 [18]. In order to explore further the conditions that could lead to brittle fractures, thermal simulations were made for a range of incident heat flux and pulse durations. The peak surface temperature (Figure 11a) contours follow those of constant heat flux factor, as they should. The heat flux factor contour of 6 MW m^{-2} $s^{1/2}$ coincides with the contour $T_{0.0}$=400°C. The bulk temperature 0.2 mm into the MB, $T_{0.2}$, (Figure 11b) remains below the DBTT when following the same heat flux factor contour. However, for lower heat fluxes and correspondingly longer pulse durations, the heat pulse has more time to diffuse into the bulk, resulting in smaller thermal gradients. Indeed, in the limit of very small heat flux and very long heating time, the temperature profile would be nearly flat and no stresses would be generated. The heat flux factor alone is therefore not enough to determine whether brittle cracking could occur. High heat flux and short pulse durations result in stronger temperature gradients (Figure 11c), which should be more efficient at producing compressive stress during the heating phase, and tensile stress during the cooling phase.

Disruptions are the most obvious source of transient heat pulses in WEST. Based on estimates from other tokamaks [24] we estimate the peak heat flux to the divertor during a thermal quench as

$$q_{pk} = f_W W_{dia}/2\pi R \, f_\lambda \lambda_q \, \Delta t \tag{1}$$

where $0.1 < f_W < 0.5$ is the fraction of the nominal thermal energy (we take W_{dia}=100 kJ as a typical value in WEST), $5 < f_\lambda < 10$ is the widening of the SOL heat flux decay length during the thermal quench (λ_q~5-15 mm in WEST [4,25,26]), and $\Delta t = (\tau_r + \tau_d)/2$ is the time scale for energy deposition on the divertor. The heat pulse to the divertor following a thermal quench has a roughly triangular waveform (see Chapter 3.2 of [27]). There is an initial fast rise of the heat flux τ_r on the time scale of the thermal quench itself which is observed to be in the range of a few 100 µs in medium-sized tokamaks such as ASDEX-Upgrade [28]. A mean value of τ_r in ASDEX-Upgrade was about 500 µs, but values as low as 100 µs (the time resolution of the infrared camera) and as high as 1 ms were observed. After peaking, the heat load decays with a time scale τ_d that is slower, up to 2 ms. The fast rise corresponds to the initial ergodization of the magnetic flux surfaces and the first connection of the PFCs to the core plasma, while the second time is likely related to the transport time of cold plasma along the field lines to the wall (i.e. the time needed to "empty" the connected flux tubes, analogous to the mechanism of heat flux deposition on the divertor during an ELM [29]).

There are no fast infrared camera measurements in WEST, so we shall assume that the time scale of thermal quenches is similar to ASDEX-Upgrade. Taking random combinations of the parameters as specified above generates a distribution of possible heat loads, 50% of which lie in the range $10 < q_{pk} < 30$ MW/m^2. For a typical B-field angle of 3°, the peak parallel heat flux would be in the range $200 < q_{//} < 600$ MW/m^2 so it seems plausible, with regards to [18] that disruptions in WEST can exceed the threshold for brittle fracturing of the exposed MB leading edges.

Another source of transient events could be large MHD crashes. Crude estimates of the associated heat flux based on Langmuir probe measurements were presented in [8], but the time scale of the phenomenon is comparable to the voltage sweep rate of the probes (1 kHz) making the analysis tricky, so work on statistical sampling is needed to obtain more precise estimates. Nonetheless, is seems plausible that large MHD crashes which result in magnetic connection of the divertor to the confined plasma could result in heat fluxes similar to those that are expected during a thermal quench that precedes a disruption.

2.5   Could the damage be caused by steady state heat loads?

During high heat flux tests, under cyclic heat loading at 20 MW/m^2 large cracks are sometimes observed at the center of MBs above the cooling tube [30,31]. They extend across the entire poloidal width of the MBs (12 mm) and can reach down to the soft copper interlayer. Elastic-plastic finite element analysis showed that strain due to toroidally-directed compressive stress in the heating phase can exceed the yield strength of tungsten and lead to

plastic deformation [32]. Poloidally-oriented crack formation (perpendicular to both the stress direction and the vertical temperature gradient) is believed to occur once the W recrystallizes to a depth of ~3 mm [33,34]. During the heating phase, the temperature decreases linearly over the 6 mm W thickness from ~ 1800°C at the top surface to ~550°C at the W-Cu interface. We shall take this gradient (dT/dz~200°C/mm) as an indication of loading conditions which can generate stresses high enough to exceed the yield strength of recrystallized W, and cause fatigue cracking.

The heat flux to the surfaces of a WEST unshaped MB was calculated by ion orbit modelling [9] on a PFU that is misaligned by 0.8 mm with respect to its upstream neighbour (Figure 12). To represent the highest performance discharges that were obtained in the WEST C3 campaign, the heat flux to the top surface was q_{pk}=2.5 MW/m^2, ion and electron temperatures were T_i=T_e=40 eV, the magnetic field was B=4 T, and its angle of incidence with the top surface was α=1.9°. The peak heat flux on the exposed leading edge was 70 MW/m^2.
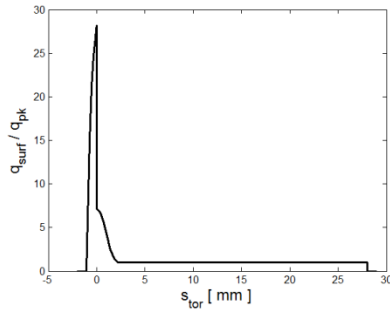

Figure 12. Toroidal profile of the heat flux to a misaligned WEST MB normalized by the heat flux to the top surface q_{pk}=2.5 MW/m^2. The leading edge is at s_{tor}=0 mm; negative values correspond to the front face inside the toroidal gap. The MB is misaligned by +0.8 mm.

The peak temperature at the exposed leading edge, Figure 13, after a 5 s exposure to this heat flux profile, attained 1726°C, above the recrystallization temperature range of W. The local temperature gradient at the leading edge was ∇T=700°C/mm. The contour on which ∇T=200°C/mm forms a quarter circle centered on the leading edge with a radius of ~2.0 mm. The temperature along that contour is ~1000°C, and is roughly at the lower bound of the expected range of recrystallization temperatures.

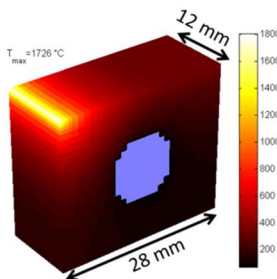Figure 13. Surface temperature of a misaligned MB exposed for 5 s to a heat flux to the top surface q_{pk}=2.5 MW/m^2. The 0.8 mm exposed leading edge is irradiated by the parallel heat flux which, when ion orbit effects are accounted for, peaks at q_{surf}=70 MW/m^2. The 3D heat flux profile from which a toroidal slice was shown in Figure 12 was used for the surface boundary condition of this thermal calculation.

This simple calculation indicates that

(1) the leading edges of misaligned monoblocks are probably recrystallized in a volume that extends ~1 mm in the toroidal and vertical directions, and

(2) the strain in that volume could potentially lead to poloidal stresses that exceed those which can lead to the macro-cracking above the cooling tube that is sometimes observed in high heat flux tests at 20 MW/m^2 (700°C/mm calculated here versus 200°C/mm calculated for the high heat flux tests).

The authors are not aware of any high heat flux tests having been conducted with steady state heat fluxes of the order of 100 MW/m^2 being applied to a narrow strip at the leading edge of an actively cooled MB. Such tests are needed to be able to draw conclusions. Nonetheless, the poloidal stresses that would be produced, if they are strong enough, would lead to the crack orientation that is observed in WEST (i.e. running downwards into the poloidal gaps, and toroidally along the top surfaces of the MBs). Elastic-plastic thermomechanical analysis such as in [22] is needed to model crack propagation in such a case. This will depend on the temperature gradients inside the MB, the accumulation of plastic deformation, and recrystallized fraction within each W grain. Given the conjectural nature of the preceding discussion, and the results of high heat flux tests on cold W that already exist, we feel that brittle fracturing is most likely responsible for the observed damage in WEST, but it would be useful and interesting to investigate, both experimentally and numerically, the effect of a huge steady state heat load onto the leading edge or onto the OHS of an actively cooled MB.

2.6 Cracks on reciprocating Langmuir probes

WEST is equipped with a mobile outboard limiter that is used to protect the RF antennas during plasma startup. Two magnetically driven reciprocating Langmuir probes are mounted on the rear face of the limiter and make brief excursions into the SOL to measure the plasma parameters [35]. The delicate internal components of the probes are protected by 2cm diameter cylindrical heat shields manufactured from W-La(10%) alloy (Figure 14a). When not in operation, the tip of the heat shield is retracted 3 mm behind the W-coated CFC armour tiles.

Most of the first year of WEST operation (C1 campaign, 2017) was spent trying to obtain a sustained plasma breakdown [36]. During that time the probes were not used. During the C2 campaign in the first half of 2018, diverted plasmas were obtained and the reciprocating probes were commissioned. They were exposed about 50 times to very tenuous and low temperature plasmas, with parallel heat flux less than 1 MW/m^2. They were impacted by 4 disruptions. Following the C2 campaign in mid 2018, the lower probe was removed to make room for another experiment, while the upper probe remained in operation for the C3 and C4 campaigns until the end of 2019. It made ~1000 reciprocations into the SOL, with heat fluxes reaching several 10s of MW/m^2 as plasma performance improved over time. It also experienced a number of disruptions. In 2020 the upper probe was removed for maintenance and that is when we learned that both probes had cracked in the same way as the divertor MBs.

On the lower probe (Figure 14c), the cracks are very thin and difficult to see even under a microscope. Assuming that the cracks on both probes developed in the same way during the C2 campaign, those on the upper probe, which was much more exposed to plasma, seem to have evolved (Figure 14b). Near the tip of the probe they have opened up and exhibit fine scale melting at their edges. The length of the cracks (~1 cm) corresponds roughly to the characteristic SOL decay length in WEST. The spacing between cracks (~0.5 mm) and their appearance are nearly identical to those observed on the exposed leading edges and OHS of the divertor MBs.
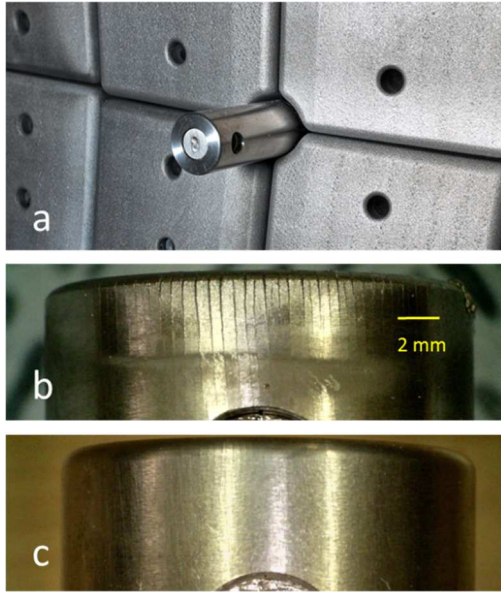

Figure 14. (a) Photograph of the lower reciprocating probe on the mobile outboard limiter before first plasma in WEST. The visible cylindrical part is a W-La(10%) heat shield. (b) The tip of the upper probe's heat shield after ~1000 reciprocations and a number of disruptions. (c) The tip of the lower probe's heat shield after only 50 reciprocations and 4 disruptions during the early phase of WEST operation (C2 campaign, 2018).

The remarkable similarity between the cracks on MBs and those on the probes suggests that they were formed the same way. The divertor's irradiation history folds in every plasma and transient event since the beginning of operation, making it impossible to draw conclusions about what caused the cracks to form. The observation of similar cracks on the lower probe that measured very weak plasma flux and experienced only 4 disruptions lends credence to the hypothesis that the cracks formed under a mode of brittle fracture. Exposure to a steady state SOL heat flux less than 1 MW/m^2 for a few tens of ms (the duration of the reciprocation) leads to a surface temperature increase of merely a few °C. The cracks, therefore, could only have been formed during the 4 disruptions. The observations of the upper probe show that once formed, and upon irradiation to higher steady state loads and increasing numbers of disruptions, the cracks evolve over time, opening up, with the appearance of localized edge melting. It is impossible to know whether the evolution is continuous, or saturates at some point. Both probes, with their respective surface states (the lower probe having barely visible cracks, and the upper probe having cracks visible to the naked eye), will be reinstalled for the next experimental campaign (C5, late 2020). The probes will be inspected between future experimental campaigns to see how the cracks on both probes evolve.

3 Conclusions

On ITER-like PFUs under modest additional heating in the WEST tokamak, cracking was observed on misaligned leading edges and optical hot spots over a broad poloidal extent of the misaligned PFU#12, but also on other PFUs that were not discussed here (see [8] for more details). MBs 8-21 at the HFS and LFS strike points and also in the private flux region exhibit cracking on both leading and trailing edges, which suggests that the cracks could have been formed during extreme strike point movements. These happen during the formation of the X-point and during ramp-down, and disruptions often occur at those times. This leads us to hypothesize that the cracks are brittle in origin, and likely occurred very early in the campaign, perhaps on the first disruption that was powerful enough to exceed the cracking threshold.

At the standard strike point positions, fine scale melting at the crack edges and deformation of the material between the cracks is observed. This could be a result of the steady state loading. The stresses can be very high at the exposed leading edge and plastic deformation could lead to the formation of the column-like structures that are seen. In addition, the material at the leading edge may be in the process of recrystallizing. The resulting degradation of the thermal properties, combined with cracks that form perpendicular to the direction of heat flow, might be responsible for the melting. At the same time, there are no experimental studies on intense steady state heating of an exposed leading edge in high heat flux devices; given the very high local temperature gradient, the resulting poloidal stress could conceivably lead to fatigue cracking. Calculations and dedicated high heat flux tests are needed.

To summarize, a hypothetical scenario that seems to fit to the observations is that brittle cracks form very early in the life of the PFU. If they never see intense steady state heat flux, then they will not evolve in time. The justification for this conjecture is that the cracks observed at the extreme poloidal extremities of the affected areas on the divertor, where intense steady state heat loads are not expected, are very thin, without much modification of the surrounding W. The cracked material at the strike point positions on the other hand, subjected to intense steady state heat loads, is further modified by repeated exposure to the parallel heat flux, and undergoes plastic deformation and melting. The damaged PFUs are presently under inspection and post-mortem analysis following the 2019 C4 experimental campaign to see whether the damaged surfaces have further evolved. The findings are too fresh to be shown here and will be reported in future work.

Two reciprocating probes made of W-La(10%) exhibit the same type of cracks as the MBs. One of the probes was not exposed to significant steady state heat flux, but experienced 4 disruptions. Fine cracks were observed. The second probe remained in the tokamak for another year and a half, and experienced at least two orders of magnitude more plasma irradiation. The cracks evolved over time, widening near the probe tip, with the formation of fine scale melting at their edges. These observations, combined with the fact that the probe's irradiation history is directly measured by the probe itself, are strong evidence that the cracks

are formed under a mode of brittle fracture, most likely during disruptions, and then evolve under steady state heat loading.

ITER MBs will not have plasma-wetted poloidal leading edges thanks to 0.5 mm toroidal beveling, but they will have OHSs [9,12]. The base operating temperature of the divertor will be 70°C [37], below the DBTT of W. Based on WEST results, if our hypothesis is correct, we can expect cracking at the OHS in the first ITER discharges. Starting in 2020, WEST Phase 2 will begin, with the progressive installation of a full W divertor featuring toroidally beveled MBs having the same geometry and the same OHSs as ITER. Monitoring the evolution of the OHSs and any long term impact of damage on plasma operation will be a high priority.

In the first phase of ITER operation (5 MA plasma current), present scaling laws predict that even with grazing B-field angles, uncontrolled ELM energies will be sufficient to largely exceed the brittle cracking threshold of the top surfaces of the tungsten monoblocks (see Figure 19 of [1]). The energy available in disruptions in WEST can produce parallel heat fluxes capable of exceeding the threshold for brittle cracking of the exposed poloidal leading edges of "cold" tungsten monoblocks having temperatures below the ductile-to-brittle transition temperature (250-350°C). The damage observed on exposed leading edges in WEST can thus be expected on the top plasma-facing surfaces of MBs in ITER at the earliest stages of operation, if uncontrolled ELMs occur, if they follow the predicted scaling law for ELM energy fluence [29], and if the heat flux strikes cold MBs. Based on decades of well-known results from high heat flux tests, the first transient event, or perhaps the first few events, will cause brittle cracking in ITER. If further submitted to steady state heat loading, the cracks could serve as seed points for the formation of plastically deformed structures accompanied by fine scale melting. These observations [8], strengthened by simple thermal analysis in this paper, constitute the first evidence for brittle cracking in a tokamak environment, and seem to be consistent with the findings of high heat flux tests. Furthermore, the observations presented here, if confirmed by post-mortem analysis, would support the affirmation in [1] that an ELM-free H-mode, or at least reliable ELM and disruption mitigation systems will be essential to protect the ITER divertor.

Acknowledgments

References

[1] R. A. Pitts, et al., Nucl. Mater. Energy **20**, 100696 (2019).
[2] J. Bucalossi et al., Fus. Eng. Des. **89** (2014) 907-912
[3] M. Firdaouss, et al., Phys. Scr. **2016**, 014012 (2016).
[4] R. Dejarnac, et al., submitted to Fus. Eng. Des. (2020).

[5] Y. Corre et al., Rev. Sci. Instrum. **89** (2018) 063508

[6] J. Gaspar et al., Fus. Eng. Des. **146** (2019) 757-760

[7] A. Grosjean, et al., 2020 Nucl. Fusion in press https://doi.org/10.1088/1741-4326/ab9fa6

[8] M. Diez, et al., Nucl. Fusion **60**, 054001 (2020).

[9] J. P. Gunn, et al., Nucl. Fusion **57**, 046025 (2017).

[10] V. Bruno, et al., Fus. Eng. Des. **146**, 115 (2019).

[11] T. Hirai, et al., Fus. Eng. Des. **127**, 66 (2018).

[12] J. P. Gunn, et al., Nucl. Fusion **59**, 126043 (2019).

[13] J. Linke, et al., J. Nucl. Mater. **258-263**, 634 (1998).

[14] A. Gervash, et al., Proceedings of the 19th Symposium on Fusion Technology, Lisbon, 499 (1996).

[15] J. H. Yu, G. De Temmerman, R.P. Doerner, R.A. Pitts, M.A. van den Berg, Nucl. Fusion **55**, 093027 (2015).

[16] T. Hirai, et al., Materials Transactions **46**, 412 (2005).

[17] M. Rieth, et al., J. Nucl. Mater. **432**, 482 (2013).

[18] M. Wirtz, et al., Nucl. Mater. Energy **12**, 148 (2017).

[19] T. Hirai, et al., J. Nucl. Mater. **390–391**, 751 (2009).

[20] G. Pintsuk, et al., J. Nucl. Mater. **417**, 481 (2011).

[21] J. W. Davis, et al., J. Nucl. Mater. **258**, 308 (1998).

[22] A. Durif, et al., Fus. Eng. Des. **138**, 247 (2019).

[23] T. Shen et al., J. Nucl. Mater. **468**, 348 (2016).

[24] V. Riccardo, et al., Nucl. Fusion **45**, 1427 (2005).

[25] N Fedorczak, et al., Phys. Scr. **2020**, 014046 (2020).

[26] J. Gaspar, et al., Fus. Eng. Des. **146**, 757 (2019).

[27] T. C. Hender, et al., Nucl. Fusion **47**, S128 (2007).

[28] G. Pautasso, et al., Proc. 31st EPS Conf. on Plasma Physics (London, UK, 2004) 28G P-4.132 (2004).

[29] T. Eich, et al., Nucl. Mater. Energy **12**, 84 (2017).

[30] G. Pintsuk, et al., Fus. Eng. Des. **88**, 1858 (2013).

[31] M. Li, et al., Fus. Eng. Des **101**, 1 (2015).

[32] T. Hirai, et al., Nucl. Mater. Energy **9**, 616 (2016).

[33] S. Panayotis, et al., Fus. Eng. Des. **125**, 256 (2017).

[34] A. Durif, et al., Fus. Eng. Des. **138**, 247 (2019).

[35] J. P. Gunn, J. -Y. Pascal, Rev. Sci. Instrum. **82**, 123505 (2011).

[36] P. Moreau, et al., IEEE Trans. Plasma Sci. **48**, 1376 (2020).

[37] F. Escourbiac, et al., Fus. Eng. Des. **146**, 2036 (2019).